

Investigation of Flow Conditioners for Compact Jet Engine Simulator Rig Noise Reduction

Michael J. Doty¹ and Henry H. Haskin²
NASA Langley Research Center, Hampton, VA, 23681

The design requirements for two new Compact Jet Engine Simulator (CJES) units for upcoming wind tunnel testing lead to the distinct possibility of rig noise contamination. The acoustic and aerodynamic properties of several flow conditioner devices are investigated over a range of operating conditions relevant to the CJES units to mitigate the risk of rig noise. An impinging jet broadband noise source is placed in the upstream plenum of the test facility permitting measurements of not only flow conditioner self-noise, but also noise attenuation characteristics. Several perforated plate and honeycomb samples of high porosity show minimal self-noise but also minimal attenuation capability. Conversely, low porosity perforated plate and sintered wire mesh conditioners exhibit noticeable attenuation but also unacceptable self-noise. One fine wire mesh sample (DP450661) shows minimal self-noise and reasonable attenuation, particularly when combined in series with a 15.6 percent open area (POA) perforated plate upstream. This configuration is the preferred flow conditioner system for the CJES, providing up to 20 dB of broadband attenuation capability with minimal self-noise.

Nomenclature

AR	=	area ratio between nozzle exit and duct area at flow conditioner location
$FCPR$	=	flow conditioner pressure ratio
K	=	pressure loss coefficient
M	=	Mach number through the flow conditioner system
M_j	=	fully-expanded jet Mach number
OPR	=	overall pressure ratio
POA	=	percent open area
γ	=	ratio of specific heats
<i>Subscript</i>		
1	=	upstream of the flow conditioner location
2	=	downstream of the flow conditioner location
a	=	ambient conditions
t	=	total quantity
s	=	static quantity

I. Introduction

Jet noise remains a major contributor to overall aircraft noise for the commercial fleet, as well as for military jet operations. As the jet noise community strives to better understand, predict, and reduce jet noise, a key factor in all of these efforts is the use of accurate jet noise measurements. Although there are a myriad of factors that need to be considered when making model scale jet noise measurements, as recent works by Ahuja¹ and Viswanathan^{2,3} effectively discuss, the current work will focus on one – rig noise and its potential reduction using flow conditioner devices.

In order to obtain high-quality, repeatable jet noise data from a model scale experimental jet facility, one must ensure rig noise does not contaminate the measurements. Rig noise can be generated from high velocity or non-uniform flow through upstream valves or piping or through bends in piping⁴. Rig noise due to combustion or flow

¹ Research Aerospace Engineer, Aeroacoustics Branch, Mail Stop 461, Senior Member AIAA.

² Engineer, Aeroacoustics Branch, Mail Stop 166.

over steps or cavities within the flow path is also possible. There are many causes of, and many potential fixes for, rig noise. In particular, the use of flow conditioning devices can be an effective method to combat internal rig noise because the devices assist in providing more uniform flow as well as a pressure drop that can reduce the flow velocity through the rig system. Nonetheless, flow conditioners also have a tendency to be an additional noise source themselves. This excess noise due to the high speed jet flow issuing through the flow conditioner is referred to as “self-noise” in the current work and must also be considered. There have been several valuable studies, such as Brown and Bridges⁵ and Harper-Bourne⁶, that systematically document the identification and mitigation of jet rig noise during the course of facility validations. Recent work by Brown, *et al.*⁷ also discusses rig noise due to a reticulated foam metal flow conditioner as part of a larger study on acoustic data quality.

Nonetheless, there have been few studies focused on the acoustic characteristics of flow conditioners for jet rig noise. One such work is that of Kinzie, *et al.*⁸ which found choked flow through the low porosity flow conditioners, and the resulting broadband shock-associated noise, to be an important contributor to the measured self-noise. This work recommended either attenuating the shock noise or avoiding it altogether through the use of a series of higher porosity flow conditioners. Furthermore, it was found that once the flow was choked, the peak frequency of the excess noise did not scale on hole diameter, and smaller holes (for the same overall porosity) exhibited lower self-noise levels. The current study builds upon these findings, taking their suggestions into consideration in the larger context of the unique challenges of the current Compact Jet Engine Simulator (CJES) design.

The upcoming aeroacoustic testing of a Hybrid Wing Body (HWB) model in the NASA Langley 14 foot x 22 foot wind tunnel includes the use of two dual stream CJES units mounted underneath the inverted model as shown in Fig. 1. The same 5.8% scale used for the airframe is also applied to the jet nozzles with the additional requirement that the upstream delivery system be sized to minimize external flow disturbances. As Fig. 2 shows, these design requirements inevitably lead to small delivery pipe diameters with multiple bends, limited area reduction between plenum and nozzle sections, and short lengths of piping between rig components. With such characteristics, the CJES has the potential for significant rig noise. Furthermore, the engine cycle to be studied will be bypass ratio (BPR) = 10, resulting in relatively low jet noise levels at the outset. Therefore, the current study investigates several flow conditioner samples to mitigate the risk of internal rig noise contaminating the CJES jet noise measurements. In addition, facility modifications to simulate an upstream point source permit the unique opportunity to measure the noise attenuation characteristics of the flow conditioners.

The primary objectives of the current work are twofold: to characterize the pressure drop, noise attenuation, and self-noise for various flow conditioner devices and combinations of devices over a range of operating conditions relevant to the new CJES as well as other jet noise facilities; and to determine the best flow conditioner design for mitigating the risk of CJES rig noise contaminating jet acoustic measurements.

The next section of this work describes the experimental procedures in detail including the facility and its modifications for the current test. In addition, instrumentation placement and processing techniques are described. The parameters of the various flow conditioner samples are also presented. Section III discusses the self-noise and attenuation measurements and the pressure drop results for the samples. Lastly, Section IV summarizes the results and discusses the conclusions.

II. Experimental Procedures

A. Facility Description

All experiments described herein took place in the NASA Langley Research Center Jet Noise Lab (JNL) within the Small Anechoic Jet Facility (SAJF). The facility is located in an enclosed building with well conditioned ambient air and consists of a single stream jet flow capable of delivering up to 1.13 kg/s of air through a 6.89 MPa air line. A Chromalox heater of 275 W is used to raise the stagnation temperature of the jet stream, in this case up to 310.9 K for consistency throughout the experiments. A 0.61 m diameter duct concentric to the nozzle provides a minimal co-flow velocity around the jet flow when operating a single speed fan in the exhaust duct. Given the nature of the current experiments and the low temperatures involved, the exhaust fan was not run for this work. The jet stream issues into an anechoic chamber with fiberglass wedges with tip-to-tip dimensions of 3.25 m high x 2.55 m wide x 3.86 m in the streamwise direction providing an anechoic environment down to 250 Hz.

For the current experiments the SAJF was modified to include a manifold and adapter flange consisting of four impinging jet tubes mounted just upstream of the turbulence control screens in the jet plenum as shown in Fig. 3a. The impinging jet concept has been successfully used to simulate a broadband noise source in other applications⁹. In this case, each of the four 9.53 mm stainless steel tubes are sealed with a welded cap of 9.53 mm solid rod that has been trimmed and drilled through resulting in a 4.76 mm diameter orifice as shown in Fig. 3b. The tubes are

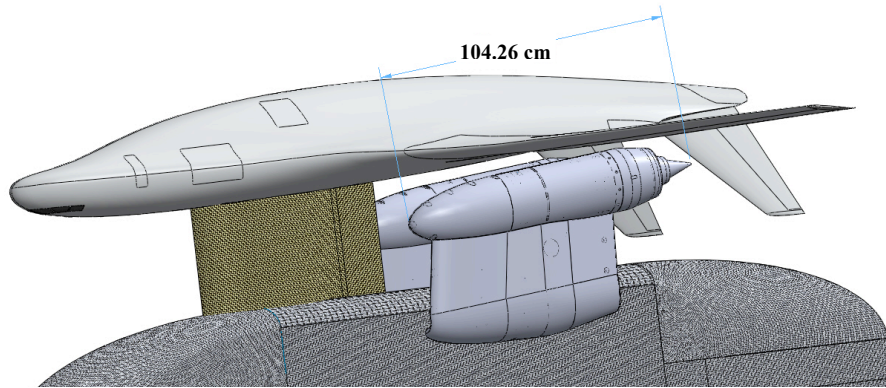


Figure 1. CJES mounted under the inverted HWB model.

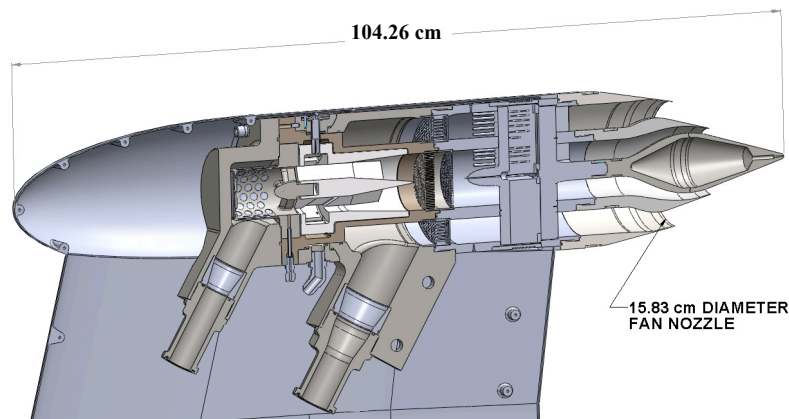
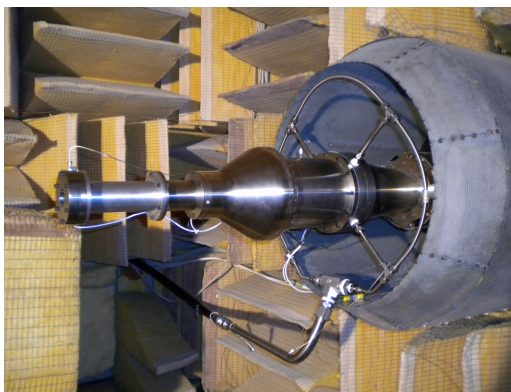
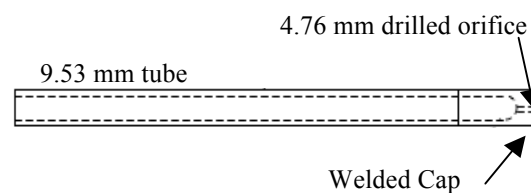


Figure 2. Compact nature of CJES rig.



a)



b)

Figure 3. Modified facility showing a) impinging jet manifold feeding into plenum and b) details of tube.

oriented 90° to one another, and the exit planes of opposing tubes are spaced 11.1 mm apart. A metered supply pressure separate from the SAJF supply is used to feed the manifold to levels up to 1.1 MPa. However, 620.5 kPa was found to be sufficient to produce a strong acoustic signature, even after attenuation, and thus was used for the

current experiments. The resulting impinging jet is a strong broadband point source that is intended to represent an upstream rig noise source to be attenuated by downstream flow conditioners.

Rather than having the piping terminate with a conventional nozzle system, the facility was further modified according to Fig. 4 to include an instrumentation flange and a 50.8 mm diameter, 88.9 mm long duct section to house the flow conditioner sample. Another duct extension of 149.2 mm length then terminates with a second instrumentation flange and an orifice plate contoured nozzle. When investigating rig noise or potential self-noise generated by flow conditioners, it is important to accurately represent the flow velocity through the rig. Therefore, not only do representative pressures need to be explored but also representative area ratios (AR) between the nozzle exit and the flow conditioner:

$$AR = \frac{A_{Nozzle\ exit}}{A_{Flow\ conditioner}}. \quad (1)$$

Consequently, three different orifice plate diameters have been tested to represent the area ratio of the CJES core stream ($AR=0.43$, $D=33.3\text{mm}$), the CJES fan stream ($AR=0.72$, $D=43.1\text{mm}$), and the Jet Engine Simulator (JES) core stream in the Low Speed Aeroacoustics Wind Tunnel (LSAWT) Facility ($AR=0.56$, $D=38.1\text{mm}$).

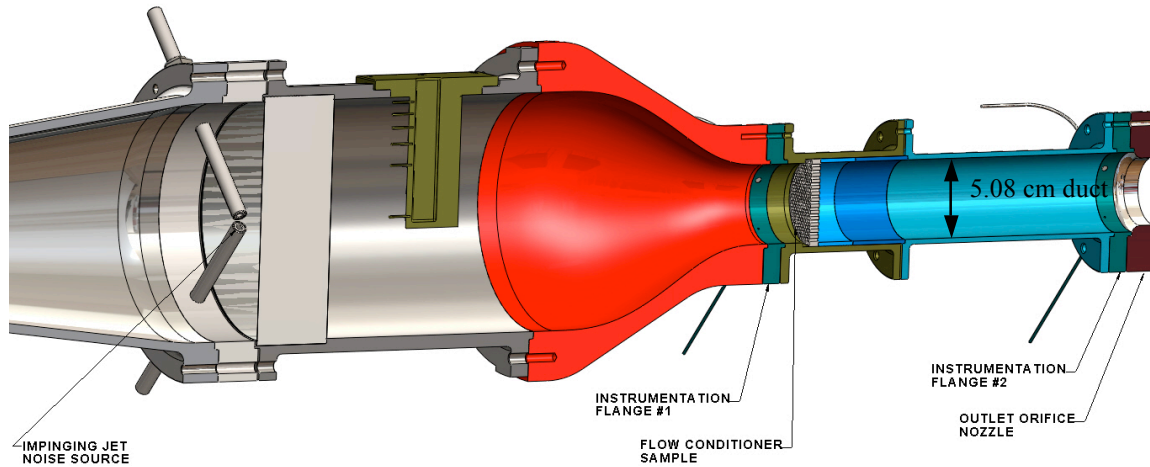


Figure 4. SAJF Facility setup for flow conditioner study.

B. Instrumentation

1. Pressure Transducers

A series of five pressure transducers were used to characterize the pressure upstream and downstream of the flow conditioner sample as shown schematically in Fig. 5. Definitions for the quantities referred to throughout this work are shown in Eqs. (2) – (4):

$$OPR = \frac{P_{t_2}}{P_a}, \quad (2)$$

$$FCPR = \frac{P_{t_1}}{P_{s_2}}, \quad (3)$$

$$\Delta P_{FC} = P_{t_1} - P_{t_2}. \quad (4)$$

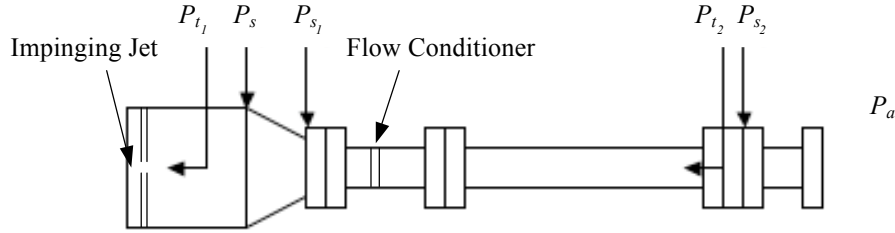


Figure 5. Schematic of pressure transducer locations.

2. Kulite Transducers

Two identical Kulite differential pressure transducers (MIC190-LT high intensity microphone series) were flush-mounted in the bottom edge (“six o’clock” position) of the upstream and downstream instrumentation flanges shown in Fig. 4. The reference ports were connected to the corresponding static pressure ports at these locations resulting in a fluctuating acoustic pressure measurement upstream and downstream of the flow conditioner.

3. Far-Field Microphones

A linear array of six Brüel and Kjær (B&K) Model 4939 free-field microphones of 6.35 mm (0.25 inch) diameter was used to measure far-field noise characteristics in conjunction with Model 2670 pre-amplifiers and a B&K Multiplexer (Model 2811). The polar range of the microphones as indicated in Table 1 was from 90° to 150° from the upstream jet axis, and the microphones were located on an azimuthal plane 32.5° above the jet centerline pointed toward the jet exit. It should be noted that to avoid measuring too far into the upper corner of the anechoic chamber, the 150° microphone was not on the same linear array as the others. Instead, it was positioned closer to the floor but still on the same azimuthal plane as the other microphones. Electrostatic and pistonphone calibrations were routinely performed on all microphones, and the grid caps were removed for testing.

C. Data Acquisition and Processing

The data acquisition system (DAS) consists of a series of LabVIEW virtual instruments running on an acquisition PC. The eight channels of dynamic signals (two Kulite and six microphone) are routed through high pass (100 Hz) and low pass (102,300 Hz) Precision filters with autogaining applied to the signals. A National Instruments PCI-6143 8 channel simultaneous sampling multi-function data acquisition (DAQ) board receives the signals. Similarly, thermocouple signals are interfaced to the DAS through a National Instruments SCXI-1102 thermocouple/voltage input module, and pressure transducer signals go through a National Instruments PCI-6122 multi-function DAQ board. The dynamic signal data are acquired at 210 kHz with 60 data averages, resulting in a 4096 point spectrum with a frequency resolution of 25.63 Hz. Far-field acoustic spectral levels are scaled to a common 3.66 m arc. While atmospheric attenuation corrections are also typically applied, the SAJF humidity sensor was not available during this test. Nonetheless, because the facility is in a controlled environment, large deviations between tests were not experienced. Based on the maximum ambient temperature difference in the anechoic chamber throughout the test, and after analyzing several possible humidity ranges at the furthest microphone location (150°), the maximum anticipated deviation between experiments due to atmospheric attenuation is expected to be less than 3 dB at 100 kHz.

D. Flow Conditioner Samples

The flow conditioners tested in the current study, as shown in Table 2, include conventional perforated plates of various thickness and porosity and laser-sintered honeycomb samples of various surface roughness, porosity, and thickness. In addition, various sintered wire meshes, felt metal, and foam metal samples were investigated. Although porosity values for the sintered wire meshes, felt metal, and foam metal were not available, approximations based on pressure drop indicate porosities typically below 20 POA for all of these samples.

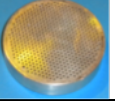
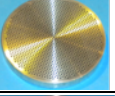
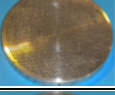
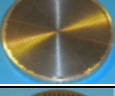
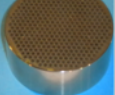
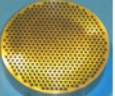
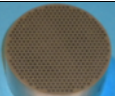
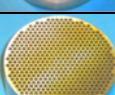
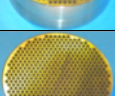
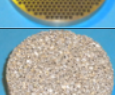



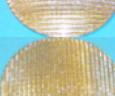

All samples have a 55.9 mm diameter and were placed in the duct which has a 2.54 mm recess to hold the samples in place. The effective diameter exposed to the flow was 50.8 mm. While porosity has been shown to be a key parameter in flow conditioner self-noise⁸, it is not clear what effect other parameters such as flow conditioner thickness or surface finish might have on acoustic performance. With laser sintering technology, a slightly defocused laser setting permitted a rougher surface finish for one sample in the current investigation. Table 2 also

shows the important characteristics of each flow conditioner and the measured pressure drop (ΔP_{FC}), pressure loss coefficient (K), and pressure ratio ($FCPR$) across each flow conditioner for a particular case of interest to be discussed. While additional pressure measurement results will be discussed in Section III C, the values included here are for convenient reference.

Table 1. Far-field microphone locations.

Microphone	1	2	3	4	5	6
Angle from upstream jet axis	90°	104°	116°	128°	140°	150°
Distance from orifice plate exit (cm)	194.06	199.64	215.65	242.57	290.83	290.83

Table 2. Flow conditioner properties.

Flow Conditioner	Photo	Geometric POA	Thickness (mm)	Further Details	FCPR at OPR=1.6, AR=0.72	ΔP_{FC} at OPR=1.6, AR=0.72
Perforated Plate		15.6	12.7	$D_{hole} = 0.889$ mm	6.18	704.65 kPa (102.2 psi) $K=2.100$
Perforated Plate		35.8	6.35	$D_{hole} = 0.889$ mm	2.85	246.33 kPa (35.7 psi) $K=1.413$
Perforated Plate		46.2	6.35	$D_{hole} = 0.889$ mm	2.20	149.86 kPa (21.7 psi) $K=1.192$
Perforated Plate		58.2	6.35	$D_{hole} = 0.889$ mm	1.86	102.67 kPa (14.9 psi) $K=1.059$
Laser-sintered honeycomb		48.3	25.4	$D_{flat-to-flat} = 1.727$ mm Average roughness	2.41	173.47 kPa (25.2 psi) $K=1.248$
Laser-sintered honeycomb		49.5	12.7	$D_{flat-to-flat} = 1.524$ mm Average roughness	2.33	132.58 kPa (19.2 psi) $K=1.096$
Laser-sintered honeycomb		56.3	25.4	$D_{flat-to-flat} = 1.626$ mm High roughness	2.15	120.65 kPa (17.5 psi) $K=1.074$
Laser-sintered honeycomb		67.4	25.4	$D_{flat-to-flat} = 1.778$ mm Average roughness	1.98	86.80 kPa (12.6 psi) $K=0.912$
Laser-sintered honeycomb		67.4	6.35	$D_{flat-to-flat} = 1.778$ mm Average roughness	1.71	52.95 kPa (7.7 psi) $K=0.734$
20 PPI Foam Metal		n/a	25.4	20 pores per inch compressed foam metal	3.68	355.06 kPa (51.5 psi) $K=1.600$
40 PPI Foam Metal		n/a	25.4	40 pores per inch compressed foam metal	3.81	300.02 kPa (43.5 psi) $K=1.519$
Felt Metal 127 w/ cross support		n/a	0.762	Sintered metal felt mesh	6.28	726.39 kPa (105.4 psi) $K=2.122$
DP 400		n/a	1.52	2 layer sintered mesh by Dynapore	7.80	935.72 kPa (135.7 psi) $K=2.378$
DP 600		n/a	1.65	2 layer sintered mesh by Dynapore	5.03	550.38 kPa (79.8 psi) $K=1.894$
DP 450661		n/a	0.457	2 layer sintered mesh 617x117 reverse Dutch weave by Dynapore	6.15	701.49 kPa (101.7 psi) $K=2.100$

III. Experimental Results

A. Flow Conditions

A range of pressure ratios representing typical subsonic and low supersonic operations was investigated in the experiments as shown in Table 3. As previously mentioned, the total temperature was held constant at 310.9 K and no co-flowing stream was used. Several broadband source pressures were also initially investigated. It was found that the 620.5 kPa provided a sufficient noise source level across a wide frequency range, and thus was used throughout the experiments. Lastly, it was decided that measurements with the broadband noise source and the jet flow would be made separately in order to properly distinguish noise attenuation characteristics and self-noise effects. This decision also permitted more consistent source levels and setpoint levels, regardless of the associated back pressure of the flow conditioner sample.

Table 3. Experimental conditions for flow conditioner measurements assuming standard atmospheric pressure.

<i>OPR</i>	<i>M_j</i>	<i>T_t</i> (K)	Mass flow (kg/s)		
			<i>AR</i> =0.43	<i>AR</i> =0.56	<i>AR</i> =0.72
1.2	0.52	310.9	0.186	0.243	0.311
1.4	0.71	310.9	0.261	0.341	0.436
1.6	0.85	310.9	0.317	0.415	0.531
1.8	0.96	310.9	0.364	0.476	0.609
2.0	1.05	310.9	0.404	0.529	0.677
2.4	1.19	310.9	0.472	0.618	0.791

B. Acoustic Measurements

Before presenting acoustic comparisons of various flow conditioners, it is useful to show the repeatability of the jet-only measurements over the course of the experiments lasting several months as new flow conditioner samples would arrive from the fabrication shop. Figure 6 shows the 90° and 150° far-field spectra for *OPR*=1.4 and the *AR*=0.43 orifice plate. As with all spectra shown in the current study, the frequency resolution is 25.63 Hz, and the sound pressure level (SPL) is referenced to 20 μPa. The 1-2 dB variability over the majority of the spectral range is indicative of a measurement uncertainty while the larger variations at the highest frequencies include the additional deviation due to differences in atmospheric attenuation as previously mentioned.

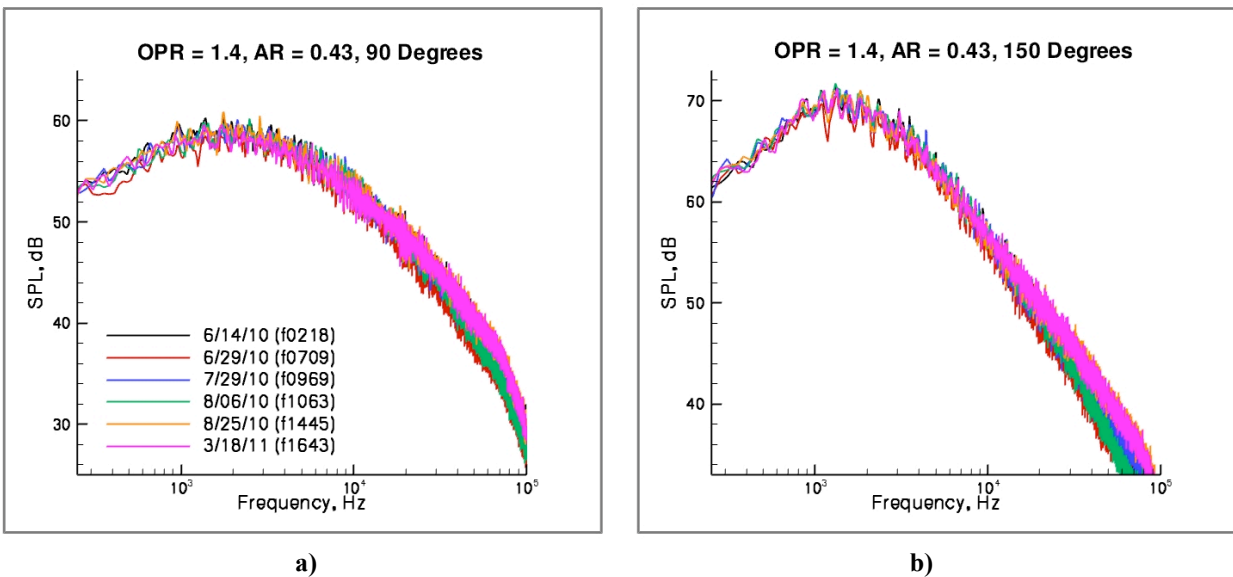


Figure 6. Repeatability measurements with no flow conditioner at a) 90° and b) 150°.

Starting with Fig. 7, the acoustic characteristics of several groups of flow conditioners are compared. The general format for the comparisons includes the far-field narrowband spectra for the jet flow only at 90° and 150° in Figs. 7a and 7b, respectively. By comparing the baseline no flow conditioner case to the others, these plots show the self-noise due to the flow conditioner in the jet flow. The data are shown for $OPR=1.6$, $AR=0.72$ because these conditions are representative of the CJES fan stream. Furthermore, the relatively low jet velocity coupled with the small area reduction (hence higher velocity through the rig) represents a particularly challenging case in terms of rig noise. Thus, if a flow conditioner with minimal self-noise at these conditions and reasonable attenuation can be found, it is reasonable to assume the flow conditioner would be as successful acoustically for the core stream conditions. This assumption will be further explored in a later plot. Figures 7c and 7d show the same far-field microphone results for the broadband source at 90 psig with no jet flow. Although the orifice plate used for the point source results is $AR=0.43$, the difference between the $AR=0.43$ and $AR=0.72$ point source results is negligible. By comparing the baseline no flow conditioner results to the other cases shown in Figs. 7c and 7d, these plots are an indication of the attenuation capabilities of the flow conditioner at the far-field observer location.

Looking more specifically now at Fig. 7, the comparisons of several perforated plate flow conditioners of various porosity, or percent open area (POA) are shown. For the 90° results of Fig. 7a the self-noise is evident above 10 kHz and increases with decreasing porosity. Referring back to Table 2, choked flow conditions ($FCPR > 1.89$) would be expected for all cases except the 58.2 POA case. Nonetheless, even unchoked cases can exhibit

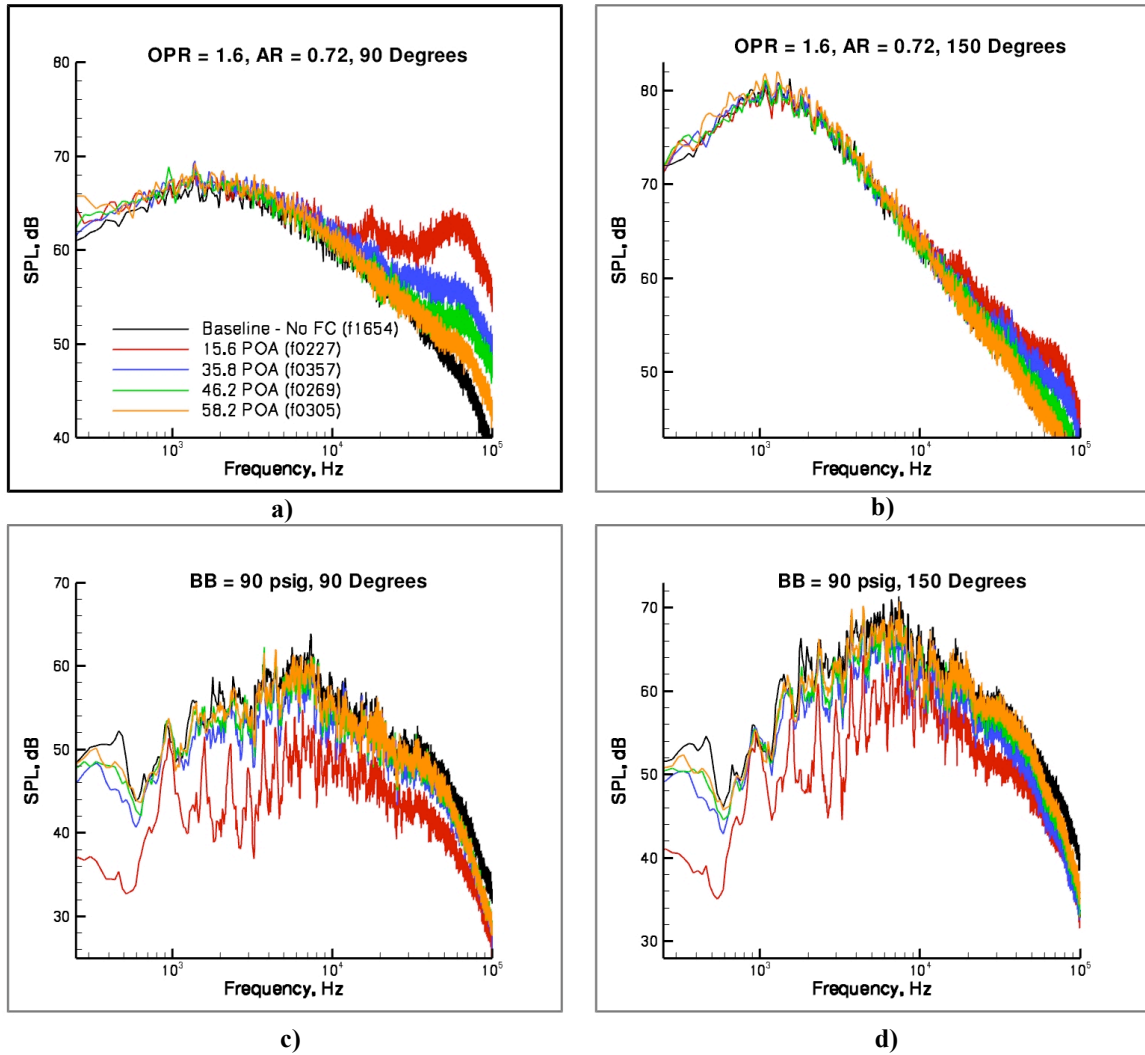


Figure 7. Perforated plate results for jet only at a) 90° and b) 150° and for the broadband source only at c) 90° and d) 150°.

excess noise due to the high speed subsonic jet flow issuing out the individual holes in the flow conditioner. In Fig. 7b, the self-noise is less evident as the low frequency jet noise levels typically dominate the spectrum at aft angles. Figures 7c and 7d show the minimal attenuation characteristics of all cases except the 15.6 POA case which exhibits approximately 5-10 dB of source noise attenuation up to 10 kHz. It should also be noted that the attenuation is less pronounced at 150° than at 90°, presumably due to the more direct acoustic ray propagation path from the source to the 150° location. The challenge from an acoustic standpoint, is to find a flow conditioner that has the capability to attenuate the upstream source without the high frequency self-noise increase.

Figure 8 shows analogous results for several honeycomb flow conditioners. With higher porosities the self-noise levels are less dramatic than in Fig. 7, but there is also minimal attenuation for any of the cases shown. It is interesting to note in Fig. 8a that the two lower porosity cases (48.3 POA and 49.5 POA) have different thicknesses, as do the two 67.4 POA cases. In both instances, the thinner flow conditioner seems to show slightly lower self-noise levels, although the slight porosity difference may be the more dominant effect in the first instance. Also, the effect of surface roughness cannot be accurately quantified because during the sample build-up, the porosity also decreased. Thus, upon closer inspection, the 67.4 POA high roughness case actually has a porosity of 56.3 POA.

Two foam metal samples are compared to the baseline in Fig. 9. While both samples exhibit self-noise at higher frequencies, the coarser 20 PPI shows a slight increase above the baseline even at lower frequencies, particularly at 150°. Incidentally, both samples show noticeable attenuation over the entire spectrum.

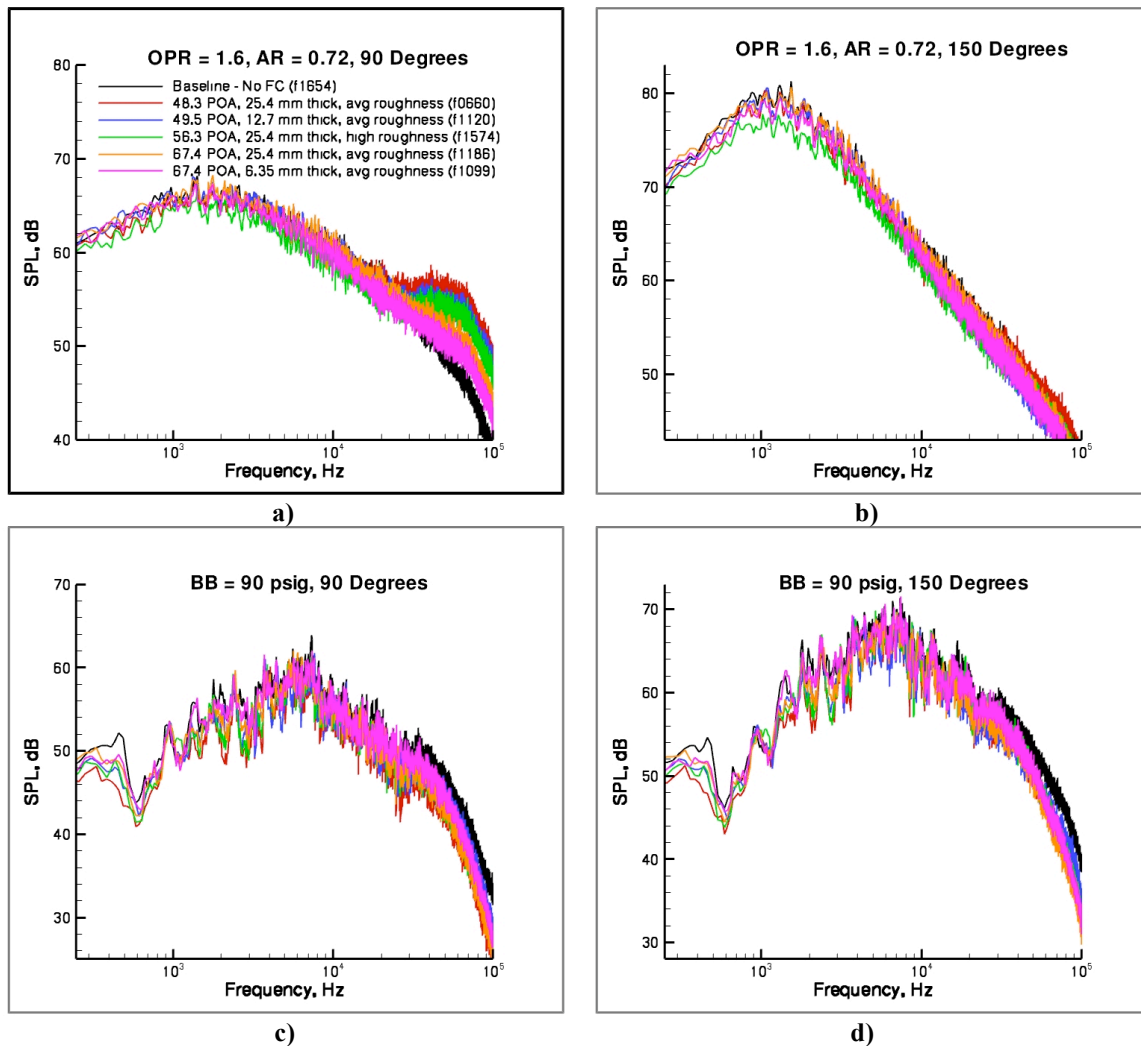


Figure 8. Honeycomb flow conditioner results for jet only at a) 90° and b) 150° and for the broadband source only at c) 90° and d) 150°.

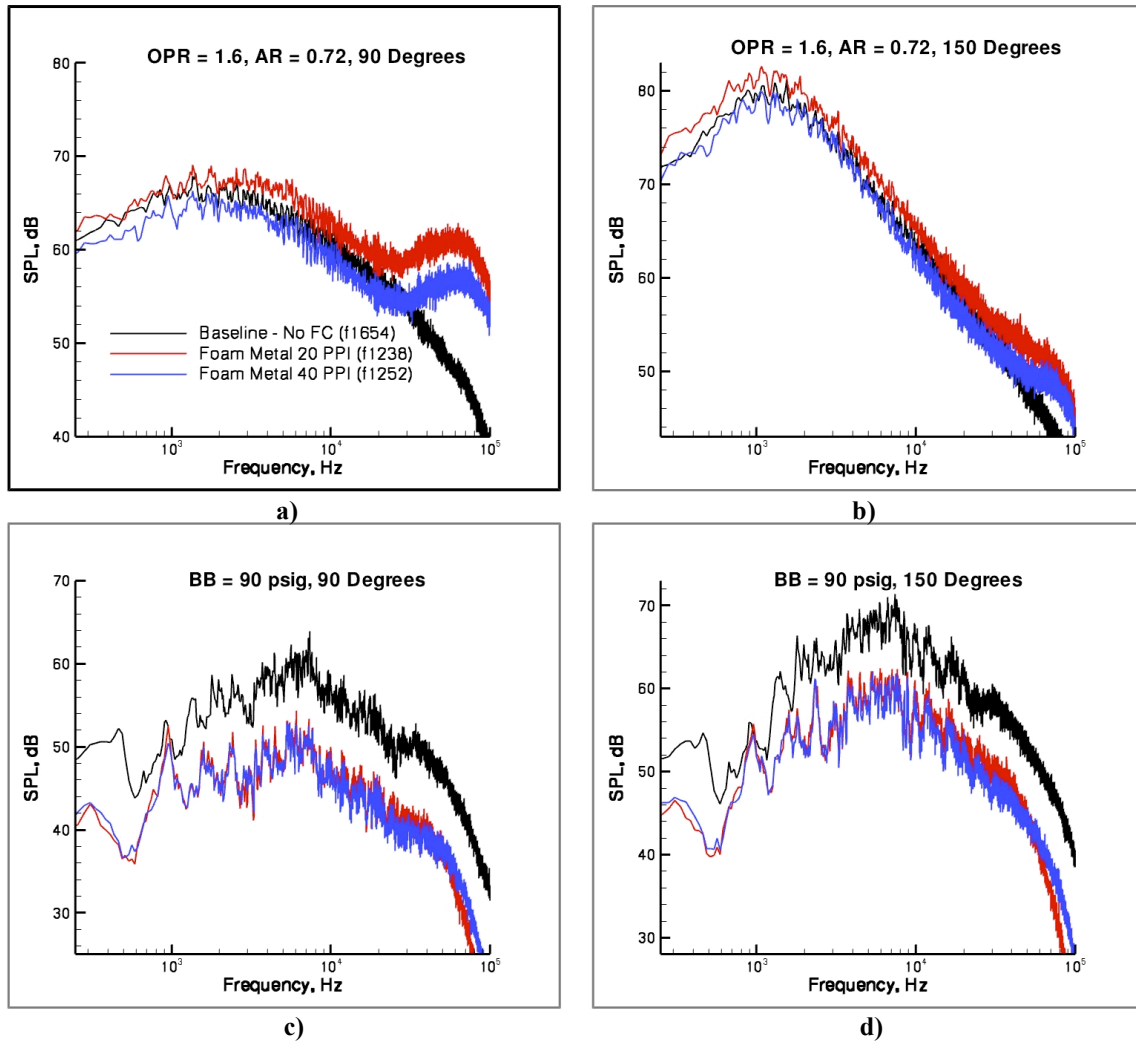


Figure 9. Foam metal results for jet only at a) 90° and b) 150° and for the broadband source only at c) 90° and d) 150°.

Several sintered wire mesh flow conditioners are shown in Fig. 10. The two thinner meshes (FM 127 and DP450661) exhibit large amplitude levels over a narrow high frequency range due to vortex shedding off the downstream cross support. However, without the cross support, the DP450661 sample shows considerable promise, as first indicated by NASA Glenn*. There is virtually no indication of self-noise and the attenuation levels are typically 8 dB or more across the frequency spectrum. If care is taken to place the finer mesh side of this sample in the downstream direction, presumably any self-noise that might be generated by the mesh is beyond the measurable frequency range. Incidentally, by flipping the sample around and having the finer mesh side face upstream, a pronounced self-noise contribution is observed in Fig. 11.

Before discussing further investigations with the best performers, the effects of staging more than one flow conditioner together are shown briefly in Fig. 12. In an effort to distribute the pressure drop over multiple flow conditioners and lower the velocity through each, several perforated plate combinations of increasing porosity are investigated, as well as one case with a perforated plate and sintered wire mesh. Figure 12 shows that although the staging helps with attenuation compared to Fig. 7, the self-noise generally takes the form of the furthest downstream flow conditioner. In fact, of the three staged cases with the 58.2 POA conditioner furthest downstream, the last two cases with a 6.35 mm space between conditioners show an increase in self-noise over the 58.2 POA alone case in Fig. 7a. However, the first staged case with a 12.7 mm spacing is comparable to Fig. 7a. These results suggest that spacing the flow conditioners too closely can have an adverse effect on the self-noise.

* Private communication with James Bridges, 1/27/10.

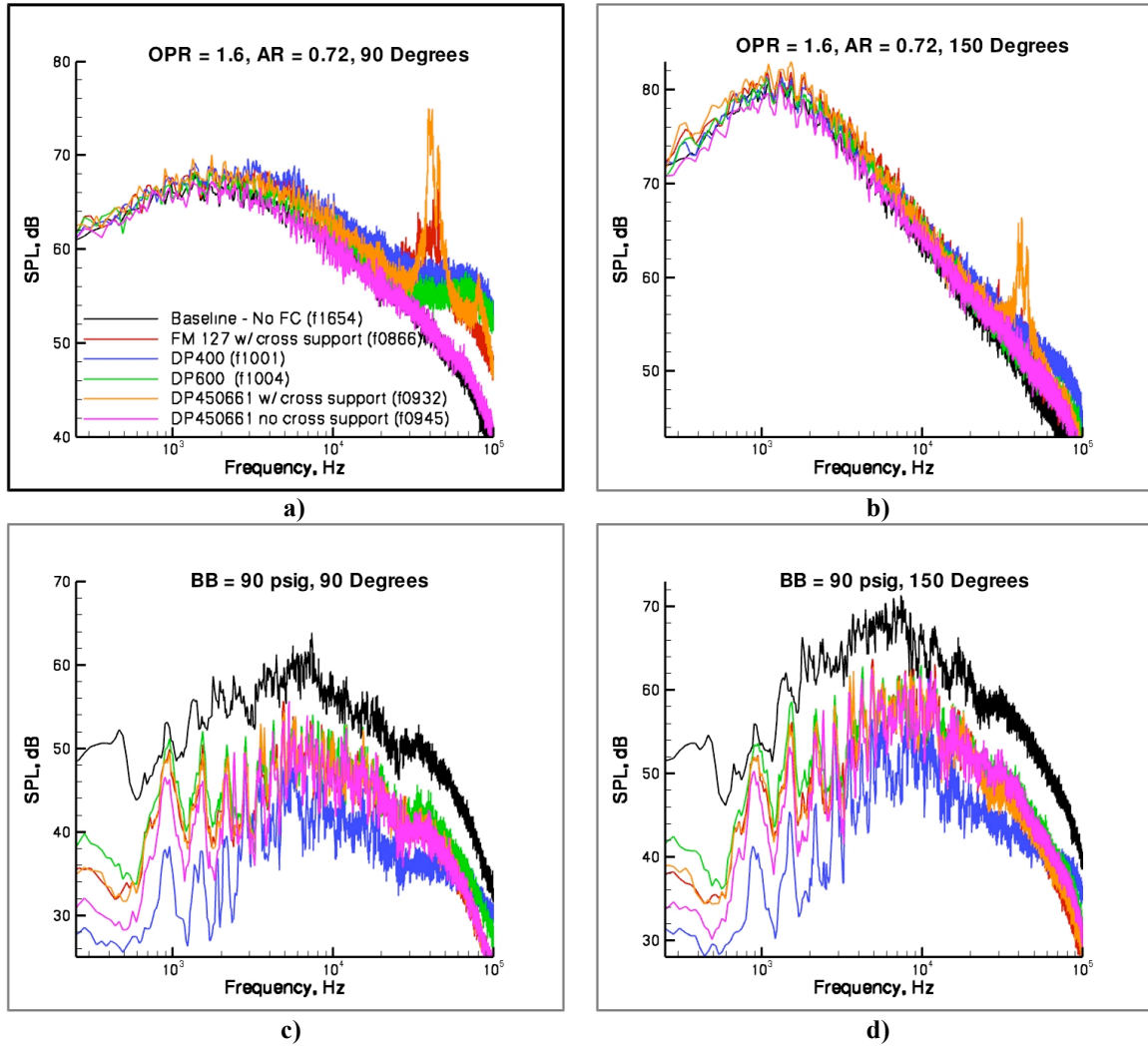


Figure 10. Sintered wire mesh results for jet only at a) 90° and b) 150° and for the broadband source only at c) 90° and d) 150°.

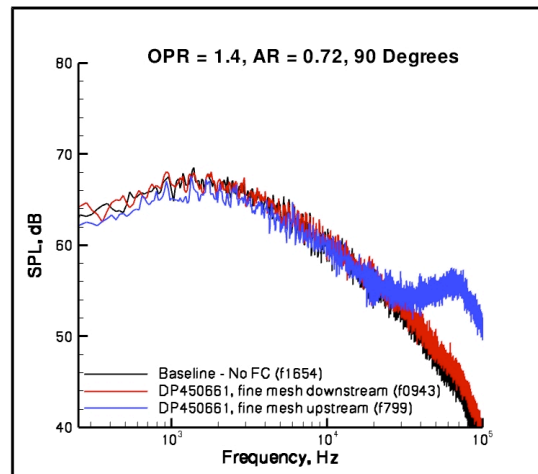


Figure 11. Influence of DP450661 fine wire mesh orientation on self-noise for jet only at 90°.

The previous results suggest the approach for an optimum flow conditioner system might be to combine a flow conditioner with good attenuation characteristics upstream with the DP450661 sintered wire mesh downstream. Yet it remains to be seen if the fine wire mesh can mitigate the self-noise from a flow conditioner upstream. Figure 13 shows that indeed, this is the case. The fine wire mesh was placed 25.4 mm downstream of the 15.6 POA perforated plate and in a separate case, 25.4 mm downstream of the 40 PPI foam metal. Both of these samples exhibit good attenuation but noticeable self-noise. Nonetheless, the fine wire mesh effectively attenuates that noise so that virtually no self-noise is seen in the far-field measurements. Because the fine wire mesh is only 0.46 mm thick, holding it in place can be an issue at high pressure drops. After several attempts, TIG welding the sample on a spacer ring yielded success, and the sample was able to stay secure throughout several cycles. The remaining case shown in Fig. 13 is an attempt to support the DP450661 with a thin, high porosity honeycomb sample butted right up against it on the downstream side. The intention is to reap the benefits of the fine mesh without the elaborate support ring. However, Fig. 13a reinforces the results from Fig. 12 in that the self-noise of the most downstream flow conditioner (in this case the 67.4 POA, 6.35 mm honeycomb sample) is still prevalent, regardless of the fine mesh upstream.

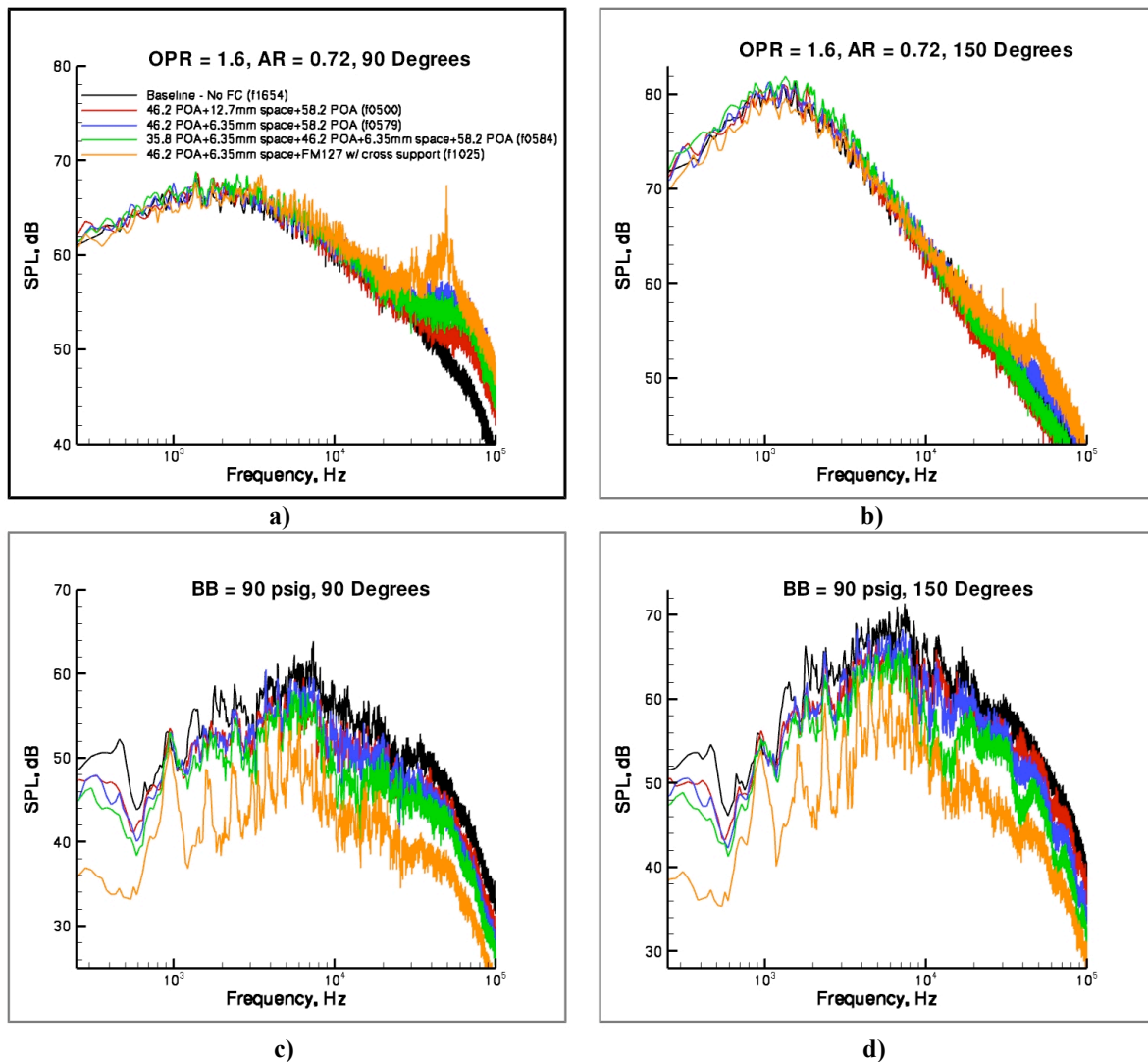


Figure 12. Staged flow conditioner results for jet only at a) 90° and b) 150° and for the broadband source only at c) 90° and d) 150°.

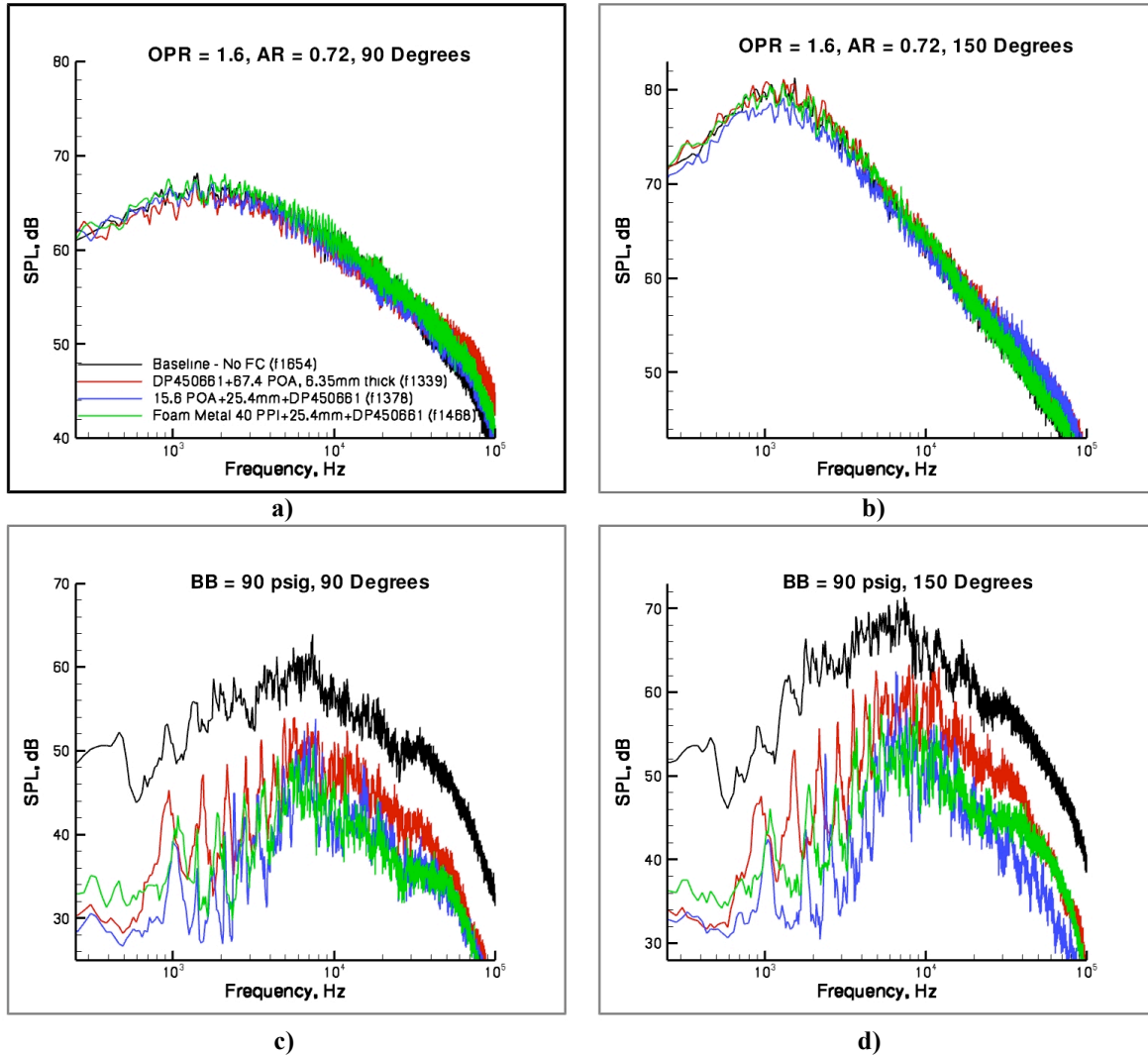


Figure 13. Combinations of best performer results for jet only at a) 90° and b) 150° and for the broadband source only at c) 90° and d) 150°.

Now that a few best case flow conditioner configurations have been explored for the CJES fan stream, it is important to check their performance for relevant CJES core stream conditions as well. Because various temperature levels were not explored during this test, the $T_t = 310.9$ K flow with $OPR=2.4$, which produces an equivalent jet velocity to the CJES core stream, will be used along with $AR=0.43$. Figure 14 shows the jet at these conditions with the same flow conditioners as in Fig. 13. Disregarding the screech tones and broadband shock-associated noise due to the imperfectly matched supersonic flow, there is still virtually no self-noise. In fact, the levels appear lower than for the baseline, particularly for the 15.6 POA/DP450661 case.

Lastly, the insertion loss for these same flow conditioners is examined with the broadband noise source in Fig. 15. Kulite measurements just upstream and downstream of the flow conditioner are shown in Figs. 15a and 15b, respectively. Figure 15c shows both upstream and downstream results for the 15.6 POA/DP450661 case. The insertion loss for these flow conditioners is over 20 db across much of the spectrum. The absence of self-noise and the significant attenuations associated with this configuration make it the preferred configuration for the CJES design.

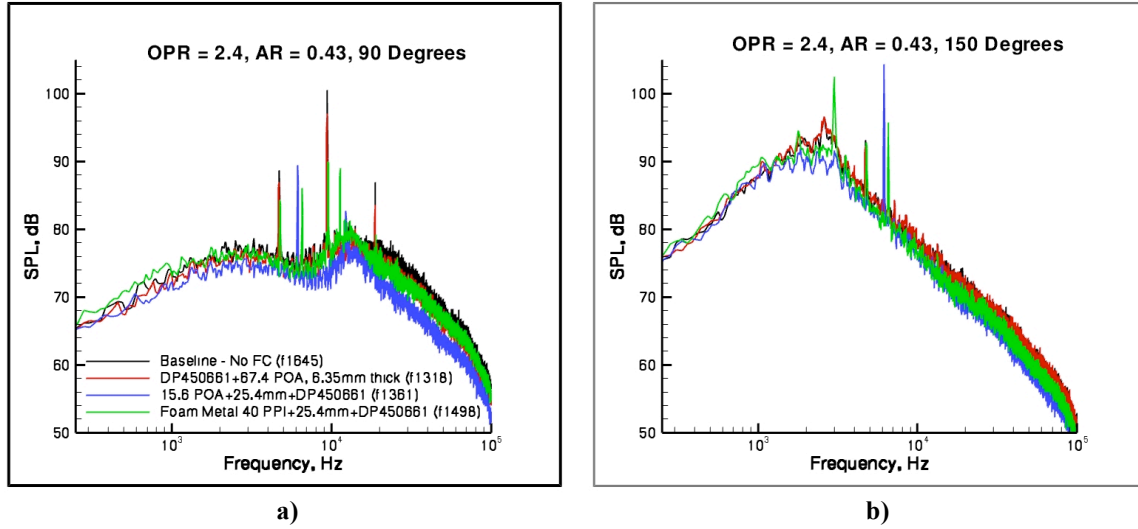


Figure 14. Best performer results for CJES core stream conditions at a) 90° and b) 150°.

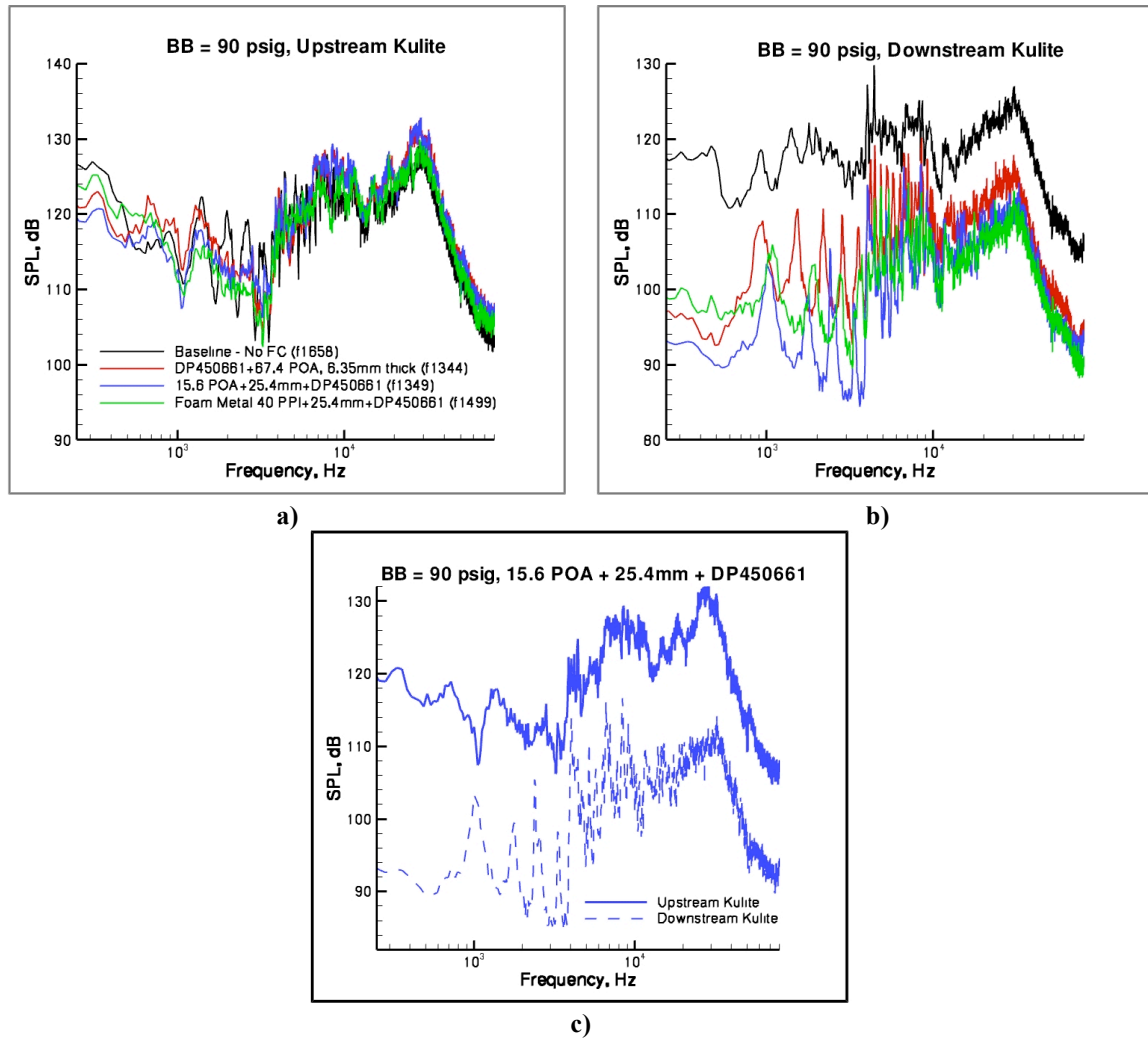


Figure 15. In-duct measurements for best performer cases a) upstream Kulite, b) downstream Kulite, and c) upstream and downstream Kulite indicating insertion loss for configuration 15.6 POA/DP450661.

C. Pressure Measurements

It is important to characterize not only the acoustic properties, but also the aerodynamic properties of the flow conditioners. Table 2 provided details of the $FCPR$ and ΔP_{FC} for each flow conditioner at the setpoint of the acoustic analysis. Nonetheless, the aerodynamic characteristics of the preferred acoustic configuration have not yet been discussed. Figure 16 shows the pressure drop associated with this configuration as a function of OPR for all the AR variations. The pressure drop becomes increasingly significant with increasing OPR and for area ratios closer to 1.0. Note that for the CJES fan setpoint ($AR=0.72$, $OPR=1.6$) this series of flow conditioners provides over 100 kPa of pressure drop. While this value is larger than any single flow conditioner in Table 2, it is considerably less than the sum of the two individual flow conditions. In fact, results from several cases indicate as long as sufficient space was maintained between two staged flow conditioners, the total pressure drop of the combination was less than the sum of the individual flow conditioners. Conversely, for the case of the honeycomb flow conditioner immediately downstream of the DP450661, the pressure drop of the staged conditioners exceeded the sum of the individual pressure drops. It should be noted that additional values of pressure drop for the $AR=0.56$ and $AR=0.72$ cases were not obtainable in Fig. 16 due to the pressure relief valve setting at 1205 kPa for these experiments.

To better model the pressure drop behavior, a pressure coefficient is calculated based on the pressure drop across the flow conditioner normalized by the dynamic pressure. While there are several variations on this procedure, the current methodology shown in Eq. (5) uses the compressible flow definition provided by Liepmann and Roshko¹⁰ and normalizes the pressure drop across the flow conditioner system by the dynamic pressure through the system:

$$K = \frac{P_{t_1} - P_{t_2}}{\frac{1}{2} \gamma P_{s_2} M^2}, \quad (5)$$

where M is the Mach number based on isentropic relations using P_{t_1} and P_{s_2} . This approach avoids using the small upstream velocities in the normalization. Figure 17 shows the pressure coefficient values for Fig. 16, as defined by Eq (5). The pressure coefficient values tend to rise with increasing OPR until $OPR=1.6$, then remain relatively constant for the ranges measured in the current work. The $AR=0.72$ curve is prematurely truncated due to the pressure relief valve setting in the experiment. With such large pressure drops expected with this flow conditioner system, a brief discussion on application to the CJES units is warranted.

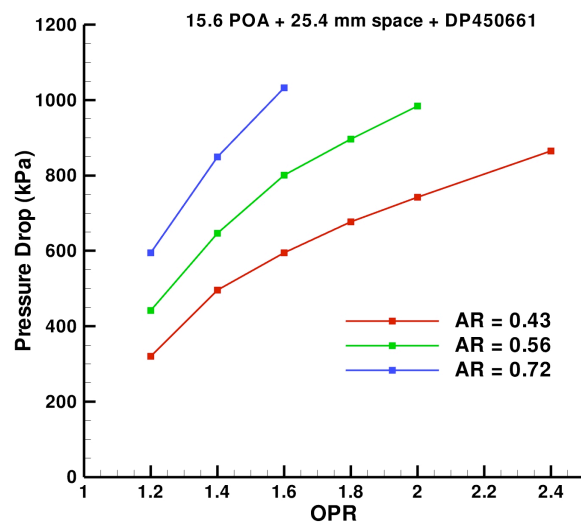


Figure 16. Pressure drop (ΔP_{FC}) for preferred configuration as a function of OPR and AR .

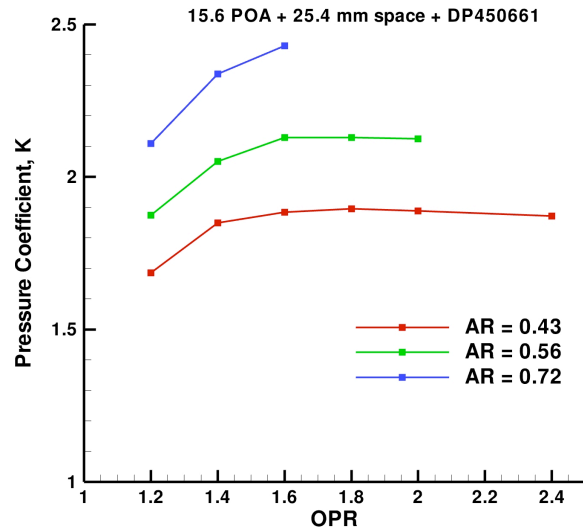


Figure 17. Pressure coefficient (K) for preferred configuration as a function of OPR and AR .

D. Application to the CJES

The demonstrated acoustic benefits of the 15.6 POA/DP450661 configuration come with the challenge of handling a large pressure drop. While the CJES design will be capable of up to 138 kPa (200 psi) pressure drop through the system, holding the thin mesh in place in the fan stream will require a welded spacer ring design similar to that used in the current experiments. Furthermore, the fine wire mesh precludes the use of seeding material for flow visualization or liquid fuel combustion applications in which unburned fuel could wick into the mesh with undesirable consequences. Although the CJES units will use gaseous propane for combustion in the core streams, it is still likely that the sintered mesh would need to be replaced often in the core stream due to thermal fatigue or perhaps be removed altogether. Additional testing with the CJES units will address these concerns more directly.

IV. Concluding Remarks

This paper characterizes the aerodynamic and acoustic properties of several flow conditioners and combinations of flow conditioners to mitigate the risk of rig noise contamination in the recently designed CJES units. Perforated plate flow conditioners of low porosity tend to attenuate upstream noise sources but exhibit self-noise at high frequencies. On the other hand, high porosity perforated plates and honeycomb devices show lower levels of self-noise but also minimal attenuation. One particular sintered wire mesh, DP450661, exhibits minimal self-noise and promising attenuation levels of up to 8 dB. When staged with a 15.6 POA perforated plate, this combination maintains minimal self-noise and up to 20 dB of broadband attenuation as long as the fine mesh is oriented downstream. Regardless of the staged configurations, the self-noise levels tend to track with the most downstream flow conditioner. Furthermore, maintaining some spacing between staged flow conditioners can help reduce self-noise and pressure drop. The relatively large pressure drop associated with the preferred configuration should be manageable for the CJES application, particularly in the cooler fan stream flow.

Acknowledgments

The authors sincerely thank the entire Jet Noise Lab team for their efforts during these experiments. M.J. Doty thanks James Bridges at NASA Glenn Research Center for the willing exchange of ideas, experiences, and additional flow conditioner samples. Finally, funding from the Environmentally Responsible Aviation Project within NASA's Integrated Systems Research Program is gratefully acknowledged.

References

- ¹Ahuja, K. K., "Designing Clean Jet-Noise Facilities and Making Accurate Jet-Noise Measurements," *Int. Journal of Aeroacoustics*, Vol. 2, No. 3&4, 2003, pp. 371-412.
- ²Viswanathan, K., "Jet Aeroacoustic Testing: Issues and Implications," *AIAA Journal*, Vol. 41, No. 9, September 2003, pp. 1674-1689.
- ³Viswanathan, K., "Best Practices for Accurate Measurement of Pure Jet Noise," *Int. Journal of Aeroacoustics*, Vol. 9, No. 1&2, 2010, pp. 145-206.
- ⁴Kuhn, G. F., and Morfey, C. L., "Noise Due to Fully Developed Turbulent Flow Exhausting from Straight and Bent Pipes," *Journal of Sound and Vibration*, Vol. 44, 1976, pp. 27-35.
- ⁵Brown, C. A., and Bridges, J. E., "Small Hot Jet Acoustic Rig Validation," NASA TM 2006-214234, April 2006.
- ⁶Harper-Bourne, M., "Commissioning and Validation of a New Jet Rig for the QinetiQ Noise Test Facility," AIAA Paper No. 2008-2958 presented at the 14th AIAA/CEAS Aeroacoustics Conference, May 2008.
- ⁷Brown, C. A., Henderson, B. S., and Bridges, J. E., "Data Quality Assurance for Supersonic Jet Noise Measurements," NASA TM 2010-216767, January 2010.
- ⁸Kinzie, K. W., Henderson, B. S., and Haskin, H. H., "Aeroacoustic Characteristics of Model Jet Test Facility Flow Conditioners," AIAA Paper No. 2005-3055 presented at the 11th AIAA/CEAS Aeroacoustics Conference, May 2005.
- ⁹Gerhold, C. H., Clark, L. R., Dunn, M. D., and Tweed, J., "Investigation of Acoustical Shielding by a Wedge-Shaped Airframe," *Journal of Sound and Vibration*, Vol. 294, 2006, pp. 49-63.
- ¹⁰Liepmann, H. W., and Roshko, A., *Elements of Gasdynamics*, John Wiley and Sons, Inc., New York, 1957, p. 55.